Acta Manilana 73 (2025), 129-144

ISSN: 0065-1370

Acta Manilana

journal homepage: https://actamanilana.ust.edu.ph/

Jackfruit (*Artocarpus heterophyllus*) Peel Biochar as Platinum-free Electrocatalyst for Oxygen Reduction Reaction in an Alkaline Medium

Philippe Andrei S. Infante[1], Hannah Grace G. Necesito[2], Bernard John V. Tongol[1,2,3,*]

[1]Department of Chemistry, College of Science;
[2]Research Center for the Natural and Applied Sciences;
[3]The Graduate School, University of Santo Tomas, Manila, Philippines 1008

Graphical Abstract

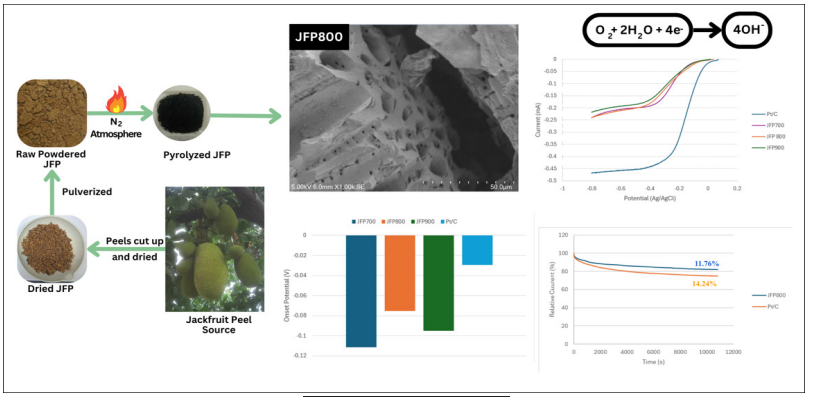

Abstract

This study explores a Pt metal-free oxygen reduction reaction (ORR) electrocatalyst prepared from jackfruit (*Artocarpus heterophyllus*) peel (JFP) biochar. The $ZnCl_2$-pre-treated peels were pyrolyzed under a nitrogen atmosphere at 700°C (JFP700), 800°C (JFP800), and 900°C (JFP900). Thermogravimetric Analysis (TGA) monitored the thermal events during the pyrolysis of the biomass, revealing the thermal stability of the resulting biochar above 600°C. X-ray Diffraction (XRD) confirmed the presence of amorphous carbon material. Scanning Electron Microscopy – Energy Dispersive X-ray Spectroscopy (SEM-EDX) revealed porous structures for all biochar samples, with an increasing amount of nitrogen as the pyrolysis temperature increased. Brunauer-Emmett-Teller (BET) analysis revealed the presence of macropores (91-96%) and mesopores (4-9%). Electrochemical characterization using Rotating Disk Electrode-Linear Sweep Voltammetry (RDE-LSV) analysis showed that all biochar-based catalysts are ORR-active in 0.1 M KOH, particularly JFP800, which demonstrated the most positive onset potential of -0.0754 V (vs. Ag/AgCl) with electron transfer number (n) of 3.5, proceeding close to the four-electron ORR pathway. Based on chronoamperometry, JFP800 was found to be slightly more electrochemically stable with a % current loss of 11.76% compared to commercial Pt/C (14.24 %).

Keywords: fuel cells, ORR, biochar, pyrolyzed jackfruit peels

Corresponding author: bvtongol@ust.edu.ph
DOI: https://doi.org/10.53603/actamanil.73.2025.ibkd7349

Date Received: 18 November 2025
Date Revised: 09 December 2025
Date Accepted: 09 December 2025

Introduction

Fuel cells are a promising alternative source of energy because they offer an avenue for renewable and clean energy. They efficiently convert the chemical energy of fuels to electricity. Additionally, they have a lower environmental impact than conventional energy conversion devices, which produce greenhouse gases mainly responsible for air pollution [1]. One of the most common types of fuel cells is the Proton Exchange Membrane Fuel Cell (PEMFC). It converts the chemical energy from the fuel source (such as hydrogen gas or liquid ethanol) to electricity through chemical reactions that occur at the anode and cathode. The anode facilitates the hydrogen oxidation reaction (HOR) or ethanol oxidation reaction (EOR), with products that include protons (H^+), which pass through the polymer electrolyte membrane and react with oxygen at the cathode, where the Oxygen Reduction Reaction (ORR) occurs [2]. Another example of a fuel cell is the Alkaline Fuel Cell (AFC), which utilizes an alkaline electrolyte, such as KOH, and operates by the movement of OH^- ions from the cathode to the anode, thereby generating energy [3]. The ORR, occurring at the cathode of the AFC, involves the following reaction:

$$O_2 + 2H_2O + 4e^- \longrightarrow 4OH^- \quad (\textit{equation 1})$$

$$O_2 + 2H_2O + 2e^- \longrightarrow HO_2^- + OH^- \quad (\textit{equation 2})$$

$$HO_2^- + 2H_2O + 2e^- \longrightarrow 3OH^- \quad (\textit{equation 3})$$

Equation 1 is the four-electron pathway [4] and is more favorable than the two-electron pathway (equations 2 and 3), which is undesirable since the product yield from this reaction is generally low.

The ORR is known to proceed sluggishly; therefore, there is a need for electrocatalysts to improve the performance of a fuel cell. Typical ORR electrocatalysts include Platinum Group Metals (PGM) [5]. Pt on carbon support (e.g., carbon black) has been the most effective electrocatalyst for ORR. Pt nanoparticles are loaded uniformly on the carbon-based surface, thus increasing the catalytic activity [6]. Despite the potential benefits of using Pt, it is not cost-effective due to its scarcity, CO deactivation, time-dependent drift, and ethanol crossover. Due to these limitations, research efforts are now focused on Pt-free electrocatalysts, with some studies demonstrating that Pt-free electrocatalysts exhibit comparable ORR activity to Pt-based electrocatalysts [7]. For instance, in the study by Mohan et al. [8], an FeGly/C catalyst was prepared by coating iron with glycine on a carbon support. The performance of the catalyst was enhanced by doping it with nitrogen, as evidenced by its higher onset potential than the undoped variant. This was also found to have an activity that is 70 mV lower than that of Pt/C. Another study by Zhao et al. [9] replaced Pt with a nitrogen-doped $LaPO_4$/C catalyst. The catalyst was found to have a better O_2 reduction peak, higher onset potential, and a more positive half-wave potential than other catalysts tested. In another study conducted by Ye et al. [10], Pt was replaced with Co on N-doped biochar support from sawdust. This catalyst exhibited a high O_2 reduction peak compared to the other catalysts, and its linear sweep voltammograms were comparable to those of other catalysts, including Pt/C. This indicates that the synthesized catalyst is suitable for the ORR.

It can also be seen that in all the Pt-free catalysts mentioned, nitrogen, a heteroatom, is an essential factor, as it alters the carbon matrix of the biochar, with N being more electronegative than C [11]. Once pyrolyzed, the biomass (which is rich in hemicellulose, cellulose, and lignin) breaks down and reacts further to form N-heterocyclic compounds, which increase the %N in the biochar.

Biochar, as a Pt-free catalyst, is an appealing sustainable source of carbon. As mentioned earlier, the presence of heteroatoms in the biochar, such as N, including S and P, may serve as dopants for the graphitic carbon nanostructures formed after pyrolysis of the biomass at high temperatures [12]. This significantly improves the catalytic activity of Pt-free ORR catalysts. For instance, Allam et al. [13] pyrolyzed water hyacinth at 900°C. The water hyacinth biochar was found to be highly porous with increased nitrogen content after pyrolysis. Additionally, the biochar remained stable over the entire CV range at which it was tested, with a high ORR reduction peak observed under basic medium.

Meanwhile, Caizán-Juanarena et al. [14] investigated the ORR activity of both hemp fibers and hemp shives in a basic medium. Both samples were pyrolyzed at 400°C, 600°C, and 800°C, then activated with KOH, and functionalized with iron phthalocyanine (FePc). It was found that hemp shives pyrolyzed at 600°C had the highest onset potential among the synthesized catalysts, with it being more positive than the values for Pt/C in literature. Another study by Matibag et al. [12] used biochar from watermelon peels pyrolyzed in a tube furnace at temperatures of 800°C, 900°C, and 1000°C under a N_2 atmosphere. The findings of the study showed that watermelon peels pyrolyzed at 1000°C gave the highest current density and the most positive onset potential using Rotating Disk Electrode-Linear Sweep Voltammetry (RDE-LSV) in acidic medium. The enhanced ORR activity may be attributed to the presence of heteroatoms S and P, aside from N, in the carbon structure, as shown by EDX analysis. Moreover, Zhang et al. [15] investigated the ORR capabilities of N-doped activated biochar (from pomelo peels) microspheres in basic solution. The onset potential for this catalyst is -0.08V, which was said to be 0.05 V lower than Pt/C. Additionally, Adios et al. [16] investigated the oxygen-reducing potential of pineapple core and pineapple crown pyrolyzed at 800°C in basic medium with onset potentials of 0.91 V and 0.95 V (vs. RHE), respectively. The pineapple core was found to be only 0.10 V less positive than Pt/C, while the crown exhibited significantly lower ORR values than Pt/C.

Kasturi et al. [17] investigated the ORR activity of jackfruit seed biochar-supported Pt. The catalyst demonstrated comparable ORR performance to commercially available Pt/C catalysts However, the ORR activity of Pt-free biochar from other jackfruit scraps, such as the peels, has not been studied thus far. Jackfruit peels have higher percent cellulose (22.78%) and percent lignin (20.41%) than other lignocellulosic biomass, such as wheat husk and rice husk [18]. It was noted that this high cellulose percentage offers good potential for bioenergy conversion. Moreover, nitrogen is innate in jackfruit peels and was observed to be higher in percentage compared to other lignocellulosic biomass, such as the ones mentioned previously. This study presents the material characteristics of jackfruit peel (JFP) biochar pyrolyzed at various temperatures and their electrocatalytic activity towards oxygen reduction reaction (ORR) in an alkaline medium.

Methodology

Preparation of Jackfruit Peels. Jackfruit peels were collected from ripe jackfruit sources in the City of San Fernando, Pampanga, Philippines. The peels were sun-dried for 36 hours, spanning six days, then further dried in an oven at 80°C for 12 hours. The dried samples were crushed using a Wiley Mill to produce the jackfruit peel powder. The powdered samples were then pre-treated with $ZnCl_2$, where 20 g of the powdered jackfruit peels were mixed with $ZnCl_2$ at a 1:1 weight ratio [19]. They were mixed with 150 mL of distilled water in a beaker with continuous stirring for 6 hours [20]. This was then filtered, and the residue was left to dry for 12 hours at 80°C.

Pyrolysis of Jackfruit Peels. This part of the methodology was adapted from Matibag et al. [12], with modifications on the pyrolysis temperatures. Four portions of the resulting JFP powder, each approximately weighing 5.00 g, were then pyrolyzed at three different temperatures (i.e., 700°C, 800°C, and 900°C) for 1 hour inside a quartz tube furnace under a N_2 atmosphere with a ramp rate of 5°C/min. The products were then allowed to cool to room temperature and were denoted as JFP700, JFP800, and JFP900. JFP700 refers to the jackfruit peel pyrolyzed at 700°C, and so on.

Characterization of Catalyst

Materials Characterization. The pyrolyzed JFP samples were characterized using SEM-EDX analysis using the Hitachi SU3800 Scanning Electron Microscope. The samples were also gold sputtered using the MC1000 ion sputter to have a better resolution for the images. Thermal Gravimetric Analysis (TGA) was performed by placing the sample in a PerkinElmer TGA 4000, which heated the sample at a rate of 5°C/min while continuously measuring the mass to assess the thermal stability of the catalyst. The Brunauer-Emmett-Teller (BET) surface area analysis was performed using the Nova Touch LX2 Surface Area & Pore Size Analyzer, which allowed N_2 gas to be adsorbed and desorbed by the sample to assess the surface area and pore volume of the catalyst. Moreover, X-ray Diffraction (XRD) was performed using the Rigaku Smartlab SE, where the sample was bombarded with X-rays at various angles, and the diffracted X-rays were detected to assess the crystallographic structure and chemical composition of the catalyst.

Electrochemical Characterization. The catalyst ink was prepared by weighing 5 mg each of the powdered JFP biochar and mixing it with 20 µL Nafion® solution (DuPont D521) and 980 µL of N, N-dimethylformamide (DMF). These were sonicated until homogeneous. To evaluate the electrochemical properties and the ORR activity of the catalyst, 1 µL of the catalyst ink was drop-casted onto a glassy carbon electrode (GCE) with an area of 0.07069 cm^2. The catalyst-coated GCE was then placed in an oven until dry. This process was repeated 10 times, resulting in a total volume of 10 µL of catalyst ink on the electrode with a catalyst loading of 0.05 mg. The GCE was used as the working electrode in cyclic voltammetry (CV) and the rotating disk electrode (RDE) in RDE-LSV. CV and RDE-LSV were performed in 0.1 M KOH, using a three-electrode setup with a Pt coil as the counter electrode and Ag/AgCl electrode as the reference electrode. The CV analyses were conducted in N_2- and O_2-purged 0.1 M KOH solutions between -0.2 V and 0.8 V at a scan rate of 50 mV/s for 10 cycles.

RDE-LSV was performed in an O_2-saturated electrolyte solution, scanning the potential from the open-circuit potential (OCP) to -0.8 V at 10 mV/s, while varying the rotation speeds from 500 rpm to 2500 rpm. To investigate the electrochemical stability of the catalysts, chronoamperometry was conducted under conditions similar to CV analyses, where -0.5 V was applied to the working electrode for 3 hours, measuring the current every 10 seconds. All electrochemical testing was performed using the Biologic VSP-300. Each electrochemical test was done in three (3) trials for each sample. Also, a freshly coated GCE was used for each trial.

Results and Discussion

Materials Characteristics of JFP biochar samples. The TGA profile (Figure 1) of the pristine JFP biomass reveals its thermal decomposition process from 50°C to 800°C, with three distinct regions characterised by varying mass losses. The initial mass loss occurs at Region 1 (70°C to 160°C) due to evaporation of moisture. It is followed by a significant mass loss, which can be attributed to the degradation of hemicellulose and cellulose (i.e., from 160°C to 390°C (Region 2)), and of lignin (i.e., from 390°C to 500°C (Region 3)) [18]. Finally, at temperatures above 600°C, the TGA profile becomes stable, with the remaining mass primarily due to carbon-rich biochar. The TGA profile from the JFP biomass is similar to the TGA profile of the jackfruit wastes, specifically, the peel and seed [18].

The XRD analysis of the JFP samples (i.e., pristine biomass and pyrolyzed samples) is shown in Figure 2. For the pristine JFP biomass, an observed diffraction peak is present at approximately $2\theta = 17°$, which could be associated to the C(101) plane from cellulose [21]. As presented in the TGA profile (Figure 1), cellulose degrades over a temperature range of approximately 160°C to 390°C. Since JFP was pyrolyzed at temperatures from 700°C to 900°C, this C(101) peak is no longer visible in the XRD patterns of the pyrolyzed samples. Both the pristine JFP biomass and pyrolyzed samples have broad diffraction peaks at around $2\theta = 22°$ and 43° corresponding to C(002) and C(001), respectively, with peak broadening being more prominent on the pyrolyzed samples. The XRD patterns of the JFP pyrolyzed samples indicate the presence of an amorphous graphite-like structure associated with the biochar [22].

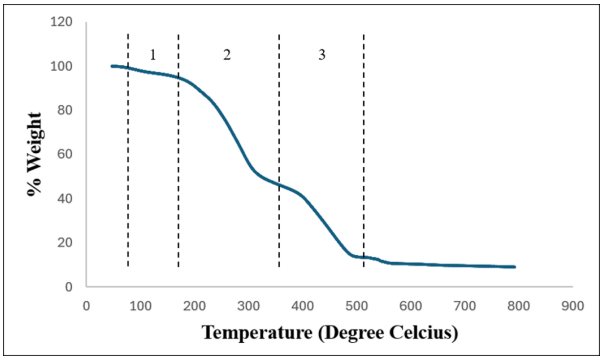

Figure 1. Thermogravimetric profile of JFP biomass showing the various regions (1-3) of thermal degradation

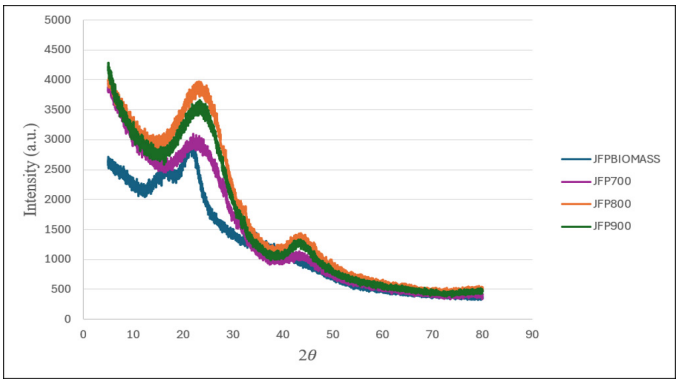

Figure 2. Powder XRD patterns of pristine JFP biomass and JFP biochar pyrolyzed at various temperature.

Figures 3 (a) and (b) show that the morphology of pristine JFP and pre-treated JFP (JFP/Zn) have smooth surfaces. Upon pyrolysis, the pores open up, revealing holes on the surfaces of JFP700, JFP800, and JFP900 as seen in Figure 3 (c) to (e). The pores are particularly visible for JFP800 (Figure 3 (d)), having large pores with smaller holes inside their walls. $ZnCl_2$ acts as a Lewis acid and a dehydration agent that selectively removes H and O from biomass, thus improving its porosity [23].

It is worth noting that after pyrolysis, the percentage of nitrogen increases, as shown in the bar graph representation (blue for nitrogen), summarizing the EDX analysis (Figure 3(f)) of the pristine, pre-treated, and pyrolyzed JFP samples. Upon degradation of hemicellulose, cellulose, and lignin via pyrolysis, an increase in % N is observed [24]. It can also be observed that the JFP800 yielded the highest percentage of N (5.4%) among the pyrolyzed samples. According to Wen et al. [25], XPS studies revealed pyridinic nitrogen in jackfruit peel biochar with a binding energy at around 399.5 eV. With this information, the nitrogen found in the EDX analysis of the pyrolyzed JFP samples could be attributed to pyridinic nitrogen. However, further XPS analysis is needed to confirm if graphitic and pyrrolic nitrogens are also present in the pyrolyzed JFP samples. Additionally, the amount of residual Zn from EDX analysis after pyrolysis is as follows: JFP700 = 5.52%; JFP800 = 0.47%; JFP900 = 0.22%. There was no complete removal of Zn done after pyrolysis. This does not pose a problem since Zn is redox-inactive, and consequently, it is not ORR-active [26].

The adsorption-desorption BET isotherms of the JFP pyrolyzed samples were also investigated. Figure 4 shows that JFP700 and JFP900 show a Type II isotherm, which is characteristic of macropores, while JFP800 shows a Type IV isotherm, since it shows a hysteresis loop. The presence of mesoporous structures, characterized by a type IV isotherm, is beneficial since it is known to enhance the ORR catalytic activity of the catalyst [27]. However, it was found that though the catalysts are all macroporous, JFP800 showed a type IV isotherm. Presumably, this could be due to the smaller pores or holes visible in the walls of the larger pores or holes of JFP800, as seen in its SEM image (Figure 3(d)). This differs from the findings of Bhushan [28], where activated carbon from JFP exhibits a type 1 isotherm, characteristic of microporous structures. This difference may be due to the pre-treatment of JFP with $ZnCl_2$ in this study.

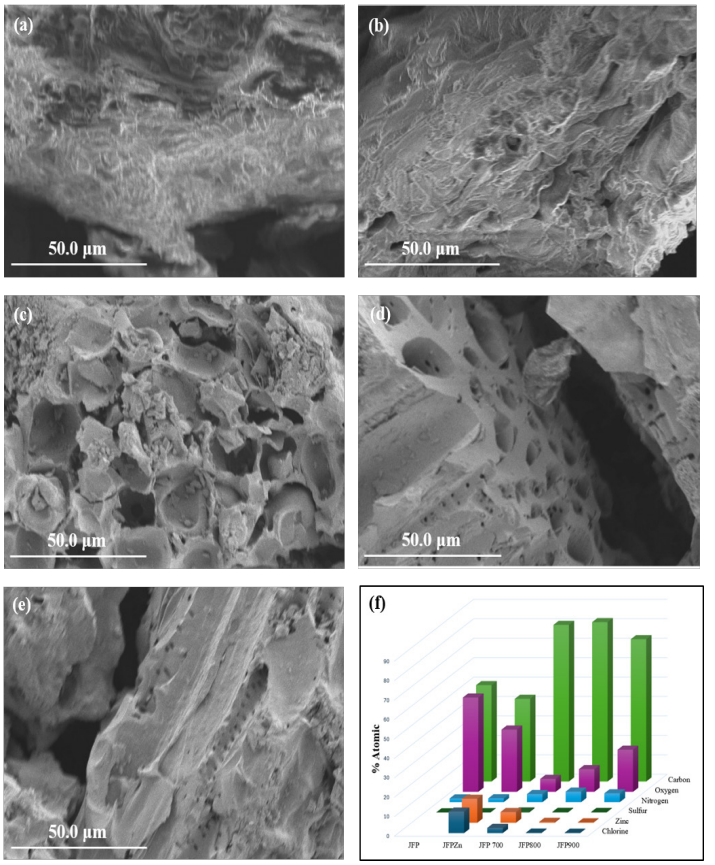

Element	JFP	JFPZn	JFP700	JFP800	JFP900
C	49.54	42.51	80.54	81.94	73.18
O	48.48	32.01	6.62	11.65	21.65
N	1.9	1.96	4.15	5.4	4.54
S	0.08	0.12	0.5	0.3	0.24
Zn	0.0	12.35	5.52	0.47	0.22
Cl	0.0	11.05	2.67	0.24	0.18

Figure 3. SEM images at 1000x magnification of (a) JFP; (b) JFP/Zn; (c) JFP700; (d) JFP800; (e) JFP900; and (f) corresponding EDX analysis of the samples

Further, the pore size distribution of the catalysts was analyzed using the Barrett-Joyner-Halenda (BJH) Method. Figure 4 (d) shows the pore size distribution curve of JFP700. The red curve, representing the differential pore volume, exhibits a sharp peak at around 1.80 to 2.00 nm, indicating that JFP700 has a small but concentrated amount of pores in this range. For the black curve, or the cumulative pore volume, there is a smooth and steady rise. This suggests that with increasing pore size, there is a continuous accumulation of pore volume. In the case of JFP800 (Figure 4(e)), the same behavior is observed for the red curve, only without the sharp peak. The difference lies in the broader distribution of this catalyst, which indicates the presence of macropores and a higher number of pores under 10 nm compared to JFP700.

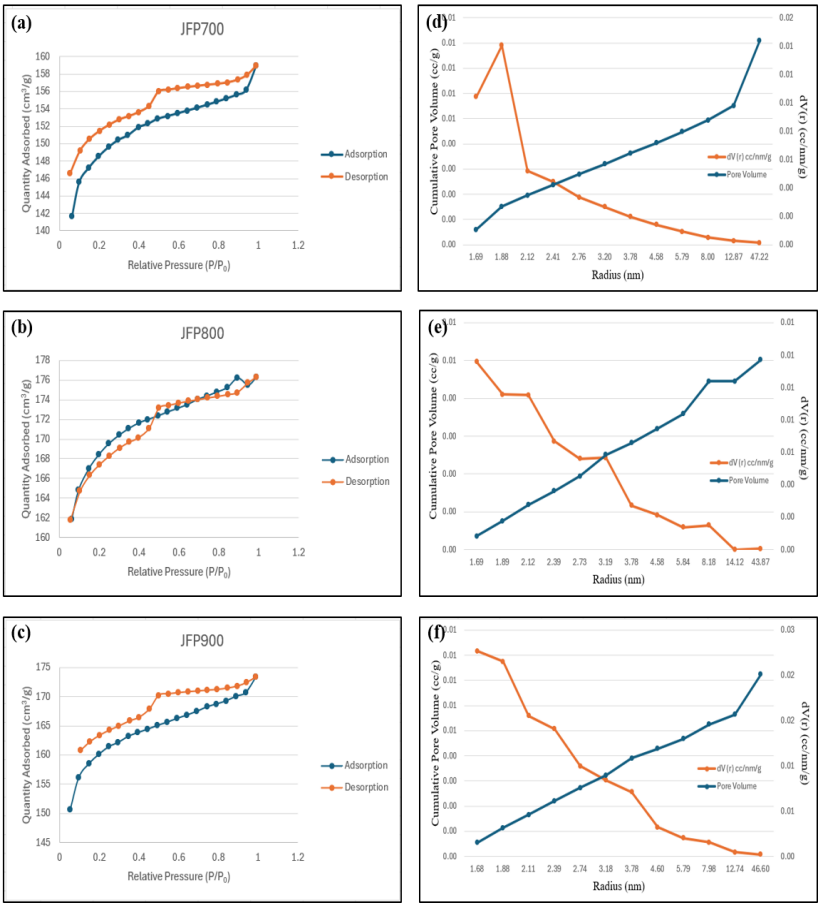

Figure 4. Adsorption-desorption BET isotherms of (a) JFP700; (b) JFP800; and (c) JFP900. BJH pore size distribution curves of (d) JFP700; (e) JFP800; and (f) JFP900.

Almost the same could be said for its black curve; the difference is that the curve flattens at around 8 to 14 nm, indicating that most pores are smaller than these values. For JFP900 (Figure 4(f)), the red curve exhibits nearly the same behavior, albeit with a narrower distribution. It also shows a similar black curve to that of JFP700.

Computing for the porosity of the catalysts, JFP700 has 94.17% macropores and 5.83% mesopores, JFP800 with 95.71% macropores and 4.28% mesopores, and JFP900 with 90.69% macropores and 9.31% mesopores. This further proves that the smaller pores or holes inside the larger pores or holes are responsible for these mesoporous behaviors in the adsorption-desorption isotherms and the BJH pore distribution curves.

From Table 1, it can be seen that JFP800 has the highest surface area and total pore volume and the lowest average pore radius, among the pyrolyzed samples. A large surface area is needed, since this would mean that more potential sites for ORR can occur, thus improving the ORR catalytic performance and stability. Notably, the average pore radii of the pyrolyzed samples fit in the macro-porous range.

Table 1. BET data of JFP pyrolyzed samples.

JFP pyrolyzed samples	Total Pore Volume (cc/g)	Average Pore Radius (nm)	Surface Area (m2/g)
JFP700	0.246	54.144	9.104
JFP800	0.273	47.801	11.439
JFP900	0.268	53.294	10.086

(Note: Standard classification for porous materials in terms of pore diameter: micropores (<2 nm), mesopores (2–50 nm), and macropores (>50 nm)). The surface area of the JFP samples is relatively lower compared to other biochar samples in literature. The surface area of the biomass is dependent on its pyrolysis conditions. However, as seen in the EDX profiles of the JFP samples, the % N increases upon pyrolysis, which enhances the ORR activity [11]. Upon decomposition of cellulose, hemicellulose, and lignin, which are proven to be in high percentages in jackfruit peels [18], they undergo a series of reactions that ultimately result in the formation of N-heterocyclic compounds [24].

Electrocatalytic Performance of JFP biochar samples towards ORR. The CV analysis of all catalysts was performed in both N_2-saturated and O_2-saturated 0.1 M KOH solutions, between -0.2 and 0.8 V at a scan rate of 50 mV/s for 10 cycles. It can be seen from Figures 5(a) to (d) that all synthesized catalysts exhibit a prominent reduction peak for the O_2-saturated electrolyte solution relative to the N_2-saturated electrolyte solution, indicating that they are all capable of catalyzing the ORR in basic medium. Figure 5 (e) presents the overlaid CVs of the O_2-saturated 0.1 M KOH solution, with all of them having peaks at around -0.4 V to -0.1 V. The commercial Pt/C still gave the most positive onset potential and the highest current density among all the catalysts investigated.

Investigating the ORR capabilities of the catalysts further, LSV was performed by scanning the potential using a Rotating Disk Electrode, from Open-Circuit Potential to -0.8 V at 10 mV/s, with varying rotation speeds ranging from 500 rpm to 2500 rpm in an O2-saturated 0.1 M KOH solution. The speeds are varied in order to obtain evenly spaced polarization curves. These speeds ensure that a uniform and stable diffusion layer is formed, allowing for a steady state to be easily achieved and enabling the polarization curves to be reproduced accurately [29]. The onset potential, half-wave potential, and current density are directly proportional to fuel cell performance metrics, such as power density [30]. For onset and half-wave potential, a more positive value indicates improved ORR performance, as it means the electrocatalyst can sustain and initiate the ORR efficiently at higher potentials, leading to reduced activation and ohmic losses. A higher current density correlates with increased capacity of delivering current without polarization losses.

Figure 6 (a) shows sigmoidal LSV polarization curves for all synthesized catalysts, including the commercial 20% Pt/C. Their sigmoidal shape shows that all catalysts are ORR-active in a basic medium. JFP800 gave the most positive onset potential (-0.0754 V) among the biochar-based catalysts. This catalyst exhibited the highest surface area (Figure 4, Table 1) and the highest percentage of nitrogen (Figure 3(e)), which may contribute to its superior ORR performance among the biochar-based catalysts.

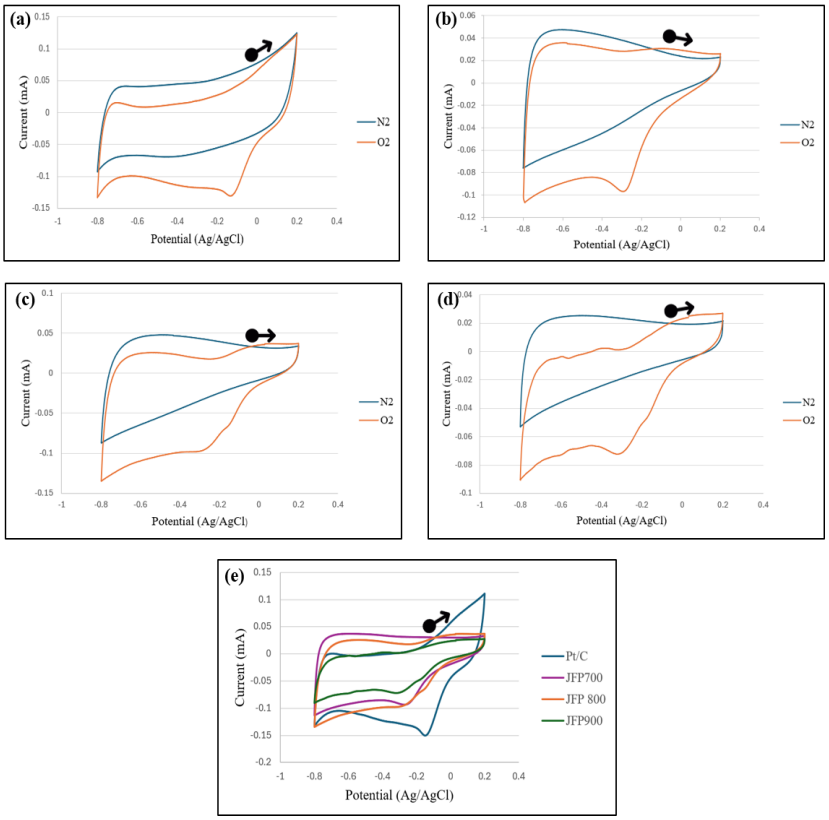

Figure 5. CV profiles of (a) commercial Pt/C; (b) JFP700; (c) JFP800; (d) JFP900 in N_2-saturated vs. O_2-saturated 0.1 M KOH; and (e) Overlaid CVs (10^{th} cycle) of O_2-saturated 0.1 M KOH at a scan rate of 50 mV/s.

However, the LSV curves of the synthesized JFP catalysts are still inferior compared to that of the commercial 20% Pt/C catalyst on the basis of the onset potential, half-wave potential, and current density (Figure 6 (a)). The Pt-based catalyst has an onset potential (-0.0294 V) which is 46 mV more positive than JFP800.

Moving further with the LSV analysis, Figure 6 (c) shows the Koutecky-Levich (K-L) plots of the JFP800 at different rotation speeds. These plots are based on the Koutecky-Levich equation as seen in equation 4, where iL is the limiting diffusion current in mA, n is the number of electrons transferred, F is the Faraday's constant (96,485 C/mol), A is the electrode area, which for this study is 0.07069 cm^2, D is the diffusion coefficient ($1.90x10^{-5}$ cm^2/s), ω is the rotation speed in rad/s, ν is the kinetic viscosity (0.01073 cm^2/s), and the c_α is the concentration of O_2 in the electrolyte (1.17×10^{-6} M) [31]. This equation relates the number of transferred electrons to the current. It is used for ORR to determine if the 4-electron or the 2-electron pathway dominates. K-L plots were made by plotting the inverse of the square root of ω against the inverse of the current density, which is the current divided by the area.

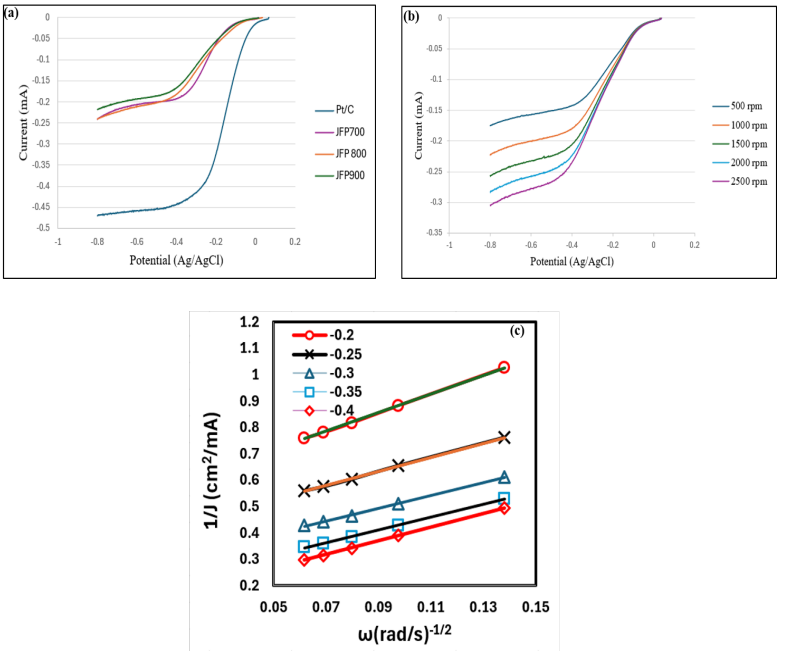

Figure 6. (a) Comparison of LSVs of all JFP-synthesized and 20% Pt/C catalysts in 0.1 M KOH at 10 mV/s and 1500 rpm; (b) Polarization curves of JFP800 from 500 to 2500 rpm at 10 mV/s and (c) K-L plots for potentials -0.2 V to -0.4 V from JFP800 polarization curves.

Five plots were created for potentials of -0.2 V, -0.25 V, -0.3 V, -0.35 V, and -0.40 V, as shown in Figure 6(c). The slopes of each plot were determined, and then calculated to obtain the number of electrons for each plot. It was determined that the mean electron transfer number (n) for JFP800 is 3.5, indicating that the 4-electron pathway of the ORR is dominant.

$$i_L = 0.620nFAD\omega^{1/2} v^{1/6} c_a \qquad \textit{(equation 4)}$$

Chronoamperometry (CA) was conducted under conditions similar to those of CV and LSV analyses, where -0.5 V was applied to the working electrode for 3 hours [27], with the current measured every 10 seconds. This is to determine how much current remains after the specified time, as a measure of the catalyst's stability. Figure 7 shows that JFP800 is more stable than Pt/C, as it exhibits a lower percentage current loss. This means that JFP800 loses less current over time than Pt/C and is more electrochemically stable.

Though the ORR performance of commercial Pt/C is still superior to JFP800 on the basis of onset potential, half-wave potential, and current density (Table 2), it is relatively less stable than JFP800 based on the % current loss. Nonetheless, the ORR performance of JFP800 is still promising, since a catalyst of such capabilities was prepared via a simple pyrolysis of jackfruit peel powder without the addition of Pt metal.

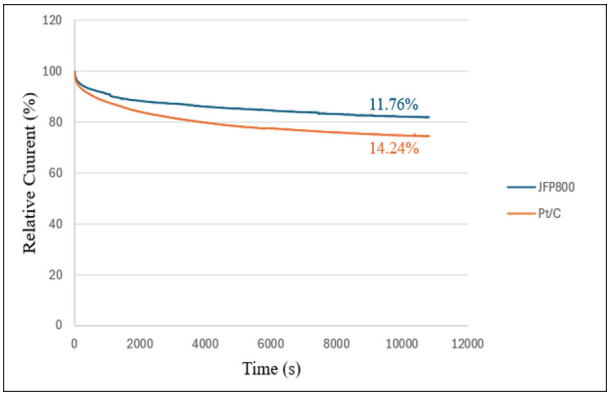

Figure 7. Chronoamperometric curves of JFP800 vs Pt/C (reported as % current loss) in 0.1 M KOH at an applied potential of -0.5 V for 10,800 s.

These results can be compared to another study [16] using pineapple core and pineapple crown, which recorded an onset potential of 0.95 V (vs. RHE) for the core and 0.91 V (vs. RHE) for the crown. The potential obtained for JFP800 was converted to the potential against RHE, since Ag/AgCl reference electrode was used in this study. The onset potential for JFP800 was calculated to be 0.89 V (vs. RHE), which is just 0.06 V and 0.02 V less positive than the pineapple crown and core, respectively. The results from this study can also be compared to the work of Li et al. [32] where the half-wave potential of watermelon peel biochar was found to be 0.72 V (vs. RHE). Following the conversion cited earlier, JFP800 has a half-wave potential of 0.71 V (vs. RHE), which is almost comparable to the watermelon peel's half-wave potential. Table 3 summarizes the ORR performance (vs. RHE) of the fruit waste-based Pt-free ORR catalysts.

Table 2. Comparison of mean ORR performance of JFP800 and commercial Pt/C in basic medium (n = 3).

ORR performance	JFP800	20% Pt/C
Onset Potential (V)	-0.0754 ± 0.0164	-0.0294 ± 0.00361
Half-wave Potential (V)	-0.2583 ± 0.0122	-0.1848 ± 0.0997
Current Density (mA/cm2)	3.42 ± 0.21	6.29 ± 0.31
% Current Loss	11.76 ± 3.01	14.24 ± 4.19

Table 3. Comparison of ORR performance (vs. RHE) of JFP800 and other fruitwaste-based Pt-free catalysts.

ORR performance (vs. RHE)	**JFP800** (This study)	**Pineapple Core** [16]	**Pineapple Core** [16]	**Watermelon Peel** [32]
Onset Potential (V)	0.89[(a)]	0.95	0.91	(b)
Half-wave Potential (V)	0.71[(a)]	(b)	(b)	0.72

N.B.: (a) Potential converted using the equation: $E_{Ag/AgCl}=E_{RHE}-0.059(pH)-E^{o}_{Ag/AgCl}$ where pH ~ 13 and $E^{o}_{Ag/AgCl}$ is 0.1976 V [27]
(b) Data not available from the cited literature.

Conclusion

This study presents a facile and cost-effective synthesis and characterization of Pt metal-free biochar-based ORR electrocatalyst via pyrolysis of $ZnCl_2$ pre-treated jackfruit peel (JFP) at different temperatures (i.e., 700°C, 800°C, and 900°C). TGA profiles showed that the synthesized catalysts are thermally stable above 600°C while XRD confirmed that the pyrolyzed products are of amorphous graphitic-like structures. SEM-EDX revealed that the synthesized JFP biochar samples are porous, with an increase in %N as the pyrolysis temperature increases. BET studies showed that these pores were found to be mostly macroporous with some mesoporous structures. CV analysis revealed that all synthesized catalysts are ORR-active in O_2-saturated 0.1 M KOH. LSV also showed sigmoidal polarization curves for pyrolyzed JFP samples in alkaline medium, with JFP800 being the best-performing ORR catalyst based on its onset potential (-0.0754 V). Additionally, the JFP800 was found to transfer 3.5 electrons, which is close to the 4-electron ORR pathway. Furthermore, the JFP800 is relatively more stable than the commercial Pt/C, as indicated by chronoamperometric analysis. This study demonstrates that agricultural wastes such as jackfruit peel can be a sustainable and low-cost source of carbon-based cathode material, which could be an alternative to the expensive Pt/C for fuel cell applications.

Acknowledgements

This study was partially supported by the Department of Science and Technology (Philippines) through the Science for Change Program – Niche Centers in the Region for Research and Development (DOST-S4CP-NICER) and monitored by the Philippine Council for Industry, Energy, and Emerging Technology Research and Development (PCIEERD) with Project No. 8881 through the research grant of B.J.V.T.

Conflict of Interest

The authors declare no conflict of interest.

Author Contributions

Conceptualization, P.A.S.I. and B.J.V.T.; methodology, P.A.S.I., H.G.G.N., and B.J.V.T.; data collection, P.A.S.I.; analysis and interpretation of data , P.A.S.I., H.G.G.N., and B.J.V.T.; original draft preparation, P.A.S.I.; review and editing of the draft, P.A.S.I., H.G.G.N., and B.J.V.T.; supervision, H.G.G.N. and B.J.V.T. All authors have read and agreed to the final version of the manuscript.

Institutional Review Board Statement

Not applicable.

Informed Consent Statement

Not applicable.

References

[1] Abdelkareem, M. A., Elsaid, K., Wilberforce, T., Kamil, M., Sayed, E. T., & Olabi, A. (2021). Environmental aspects of fuel cells: A review. Science of the Total Environment, 752, 141803. https://doi.org/10.1016/j.scitotenv.2020.141803

[2] Alias, M. S., Kamarudin, S., Zainoodin, A. M., & Masdar, M. S. (2020). Active direct methanol fuel cell: An overview. International Journal of Hydrogen Energy, 45(38), 19620–19641. https://doi.org/10.1016/j.ijhydene.2020.04.202

[3] Ferriday, T., & Middleton, P. H. (2021). Alkaline fuel cell technology - A review. International Journal of Hydrogen Energy, 46(35), 18489–18510. https://doi.org/10.1016/j.ijhydene.2021.02.203

[4] Talukder, N., Wang, Y., Nunna, B. B., & Lee, E. S. (2022). An In-depth exploration of the electrochemical oxygen reduction reaction (ORR) phenomenon on Carbon-Based catalysts in alkaline and acidic mediums. Catalysts, 12(7), 791. https://doi.org/10.3390/catal12070791

[5] Tian, X., Lu, X., Xia, B. Y., & Lou, X. W. D. (2020). Advanced electrocatalysts for the oxygen reduction reaction in energy conversion technologies. Joule, 4(1), 45–68. https://doi.org/10.1016/j.joule.2019.12.014

[6] Yu, Y., Chen, K., Wu, Q., Zhang, Y., Shi, D., & Li, H. (2023). Recent progress on reduced graphene oxide supported Pt-based catalysts and electrocatalytic oxidation performance of methanol. International Journal of Hydrogen Energy, 48(5), 1785–1812. https://doi.org/10.1016/j.ijhydene.2022.10.021

[7] Bhatt, M. D., & Lee, J. Y. (2020). Advancement of platinum (Pt)-Free (Non-Pt precious metals) and/or Metal-Free (Non-Precious-Metals) electrocatalysts in Energy Applications: A Review and Perspectives. Energy & Fuels, 34(6), 6634–6695. https://doi.org/10.1021/acs.energyfuels.0c00953

[8] Mohan, R., Modak, A., & Schechter, A. (2021). Plasma-Modified FeGly/C as a Pt-Free stable ORR electrocatalyst in an acid electrolyte. ACS Applied Energy Materials, 4(1), 564–574. https://doi.org/10.1021/acsaem.0c02452

[9] Zhao, R., Chen, Z., Li, Q., Wang, X., Tang, Y., Fu, G., Li, H., Lee, J., & Huang, S. (2022). N-doped $LaPO_4$: An effective Pt-free catalyst for electrocatalytic oxygen reduction. Chem Catalysis, 2(12), 3590–3606. https://doi.org/10.1016/j.checat.2022.11.008

[10] Ye, Y., Qian, T., & Jiang, H. (2020). Co-loaded N-doped biochar as a high-performance oxygen reduction reaction electrocatalyst by combined pyrolysis of biomass. Industrial & Engineering Chemistry Research, 59(35), 15614–15623. https://doi.org/10.1021/acs.iecr.0c03104

[11] Matos, R., Fernandes, A. J., Abdelkader-Fernández, V. K., Peixoto, A. F., & Fernandes, D. M. (2024). High performance metal-free N/S-doped biochars towards oxygen reduction reaction. Biomass and Bioenergy, 193, 107523. https://doi.org/10.1016/j.biombioe.2024.107523

[12] Matibag, V. K. R., Geronimo, H. G., Garcia, J. L., & Tongol, B. J. V. (2019). Platinum-free electrocatalyst for oxygen reduction reaction derived from the direct pyrolysis of watermelon peels. International Journal of Integrated Engineering/International Journal of Integrated Engineering, 11(7). https://doi.org/10.30880/ijie.2019.11.07.023

[13] Allam, F., Elnouby, M., El–Khatib, K., El-Badan, D. E., & Sabry, S. A. (2020). Water hyacinth (Eichhornia crassipes) biochar as an alternative cathode electrocatalyst in an air-cathode single chamber microbial fuel cell. International Journal of Hydrogen Energy, 45(10), 5911–5927. https://doi.org/10.1016/j.ijhydene.2019.09.164

[14] Caizán-Juanarena, L., Boventi, M., Muhyuddin, M., Caporali, S., Berretti, E., Lavacchi, A., Staffolani, A., Mauri, M., Simonutti, R., & Santoro, C. (2025). Hemp stem derived platinum metal-free electrocatalysts for oxygen reduction reaction in alkaline electrolyte. Electrochimica Acta, 146094. https://doi.org/10.1016/j.electacta.2025.146094

[15] Zhang, Y., Deng, L., Hu, H., Qiao, Y., Yuan, H., Chen, D., Chang, M., & Wei, H. (2019). Pomelo peel-derived, N-doped biochar microspheres as an efficient and durable metal-free ORR catalyst in microbial fuel cells. Sustainable Energy & Fuels, 4(4), 1642–1653. https://doi.org/10.1039/c9se00834a

[16] Adios, C.G., Hamid, F.H., Safira, A.N., Irmawati, Y., Sumboja, A. (2022) Pineapple waste-derived carbon as a metal free catalyst in zinc-air battery. 7th Int Conf Elect Vehicular Technology, Bali, Indonesia, 60–65. https://doi.org/10.1109/ICEVT55516.2022.9924880

[17] Kasturi, P. R., Arunchander, A., Kalpana, D., & Selvan, R. K. (2019). Bio-derived carbon as an efficient supporting electrocatalyst for the oxygen reduction reaction. Journal of Physics and Chemistry of Solids, 124, 305–311. https://doi.org/10.1016/j.jpcs.2018.08.019

[18] Alves, J. L. F., Da Silva, J. C. G., Mumbach, G. D., Di Domenico, M., Da Silva Filho, V. F., De Sena, R. F., Machado, R. A. F., & Marangoni, C. (2020). Insights into the bioenergy potential of jackfruit wastes considering their physicochemical properties, bioenergy indicators, combustion behaviors, and emission characteristics. Renewable Energy, 155, 1328–1338. https://doi.org/10.1016/j.renene.2020.04.025

[19] Chaudhary, R., Maji, S., Shrestha, R. G., Shrestha, R. L., Shrestha, T., Ariga, K., & Shrestha, L. K. (2020). Jackfruit Seed-Derived nanoporous carbons as the electrode material for supercapacitors. C – Journal of Carbon Research, 6(4), 73. https://doi.org/10.3390/c6040073

[20] Nirmaladevi, S., & Palanisamy, P. N. (2021). Adsorptive behavior of biochar and zinc chloride activated hydrochar prepared from Acacia leucophloea wood sawdust: kinetic equilibrium and thermodynamic studies. Desalination and Water Treatment, 209, 170–181. https://doi.org/10.5004/dwt.2021.26515

[21] Brahma, R., Ray, S., Nayak, P. K., & Shridhar, K. (2025). Sustainable valorization of jackfruit peel waste: Bio□functional and structural characterization. Food Bioengineering, 4, 1, 88-100. https://doi.org/10.1002/fbe2.70004

[22] Rañoa, M.E.R., Villanueva, M.L., Laxamana, J.R.P., Necesito, H.G.G., Tongol, B.J.V. (2024). Palladium/Coconut husk biochar composite material as an effective electrocatalyst for ethanol oxidation reaction, Advances in Natural Sciences: Nanoscience and Nanotechnology, 15, 025003. https://doi.org/10.1088/2043-6262/ad3de0

[23] Zhao, H., Zhong, H., Jiang, Y., Li, H., Tang, P., Li, D., & Feng, Y. (2022b). Porous $ZnCl_2$-activated carbon from shaddock peel: methylene blue adsorption behavior. Materials, 15(3), 895. https://doi.org/10.3390/ma15030895

[24] Ma, J., Ye, Z., Zhou, J., Hu, Z., Wang, Q., Wang, J., Pan, Z., & Hu, M. (2024). Co-pyrolysis of soybean straw and spirulina platensis for N-containing chemicals and N-doped carbon materials production: Unraveling the nitrogen migration mechanism and involved chemical reactions. Journal of Analytical and Applied Pyrolysis, 181, 106641. https://doi.org/10.1016/j.jaap.2024.106641

[25] Wen, Q., Chen, Y., Rao, X., Yang, R., Zhao, Y., Li, J., Xu, S., & Liang, Z. (2022). Preparation of magnesium ferrite-doped magnetic biochar using potassium ferrate and seawater mineral at low temperature for removal of cationic pollutants. Bioresource Technology, 350, 126860. https://doi.org/10.1016/j.biortech.2022.126860

[26] Hübner, C., & Haase, H. (2021). Interactions of zinc- and redox-signaling pathways. Redox Biology, 41, 101916. https://doi.org/10.1016/j.redox.2021.101916

[27] Necesito, H. G. G., Garcia, J. L., Dzmarado, E. S., Miyao, T., Inukai, J., & Tongol, B. J. V. (2025). Pyrolyzed iron-cobalt/polypyrrole/reduced graphene oxide as an effective cathode electrocatalyst for oxygen reduction reaction in an alkaline medium. Journal of Physics and Chemistry of Solids, 112556. https://doi.org/10.1016/j.jpcs.2025.112556

[28] Bhushan, B., Nayak, A., & Kotnala, S. (2021). Green synthesis of highly porous activated carbon from jackfruit peel: Effect of operating factors on its physico-chemical characteristics. Materials Today: Proceedings, 44, 187–191. https://doi.org/10.1016/j.matpr.2020.08.554

[29] Li, S., Shi, L., Guo, Y., Wang, J., Liu, D., & Zhao, S. (2024). Selective oxygen reduction reaction: mechanism understanding, catalyst design and practical application. Chemical Science, 15(29), 11188–11228. https://doi.org/10.1039/d4sc02853h

[30] Nandan, R., Bisen, O. Y., & Nanda, K. K. (2021). The untold tale of the ORR polarization curve. The Journal of Physical Chemistry C, 125(19), 10378–10385. https://doi.org/10.1021/acs.jpcc.1c02026

[31] Survila, A. (2025). On the application of Koutecky–Levich analysis to electrochemical processes involving metal complexes. 1. Theoretical background. Chemija, 36(1). https://doi.org/10.6001/chemija.2025.36.1.3

[32] Li, L., Wu, Z., Zhang, J., Zhao, Y., & Shao, G. (2021). Watermelon peel-derived nitrogen-doped porous carbon as a superior oxygen reduction electrocatalyst for Zinc-Air batteries. ChemElectroChem, 8(24), 4790–4796. https://doi.org/10.1002/celc.202101339